Paper published on:
Solar Energy Materials and Solar Cells vol. 155 (2016), pages: 368–377
DOI: 10.1016/j.solmat.2016.06.028
http://www.sciencedirect.com/science/article/pii/S0927024816302033

Process and composition dependence of optical properties of zirconium, hafnium and tantalum borides for solar receiver applications

Elisa Sani*[a], Luca Mercatelli[a], Marco Meucci[a], Laura Silvestroni[b], Andrea Balbo[b], Diletta Sciti[b]

[a]*CNR-INO National Institute of Optics, Largo E. Fermi, 6, I-50125 Firenze, Italy*
[b]*CNR-ISTEC,Institute of Science and Technology for Ceramics, Via Granarolo 64, I-48018 Faenza (Italy)*
**Corresponding author, email: elisa.sani@ino.it*

ABSTRACT

Ultra-high temperature boride ceramics have proved to show promising properties for novel solar receivers. The present work shows a further step towards their actual application, investigating how sintering technique and starting powders composition affect the properties of final materials. Thus we report on the comparative characterization of ZrB_2, HfB_2 and TaB_2 produced by high pressure and pressureless techniques and with different amounts of $MoSi_2$ sintering aid. We investigate microstructural, mechanical and optical properties, in the perspective to assess the material potential for novel solar absorbers operating at higher temperatures than those currently available. Moreover, a systematic study has been carried out on ZrB_2, producing with fixed high pressure sintering technique, a series of samples with $MoSi_2$ compositions in the range 5-50 vol%. We show that the content of silicide and silicide-related secondary phases in the final pellets affects either the mechanical performance and the optical behaviour. Thus, as far as the optical properties are concerned, the $MoSi_2$ amount should be the lowest as possible to ensure a proper material consolidation whilst enhancing the absorbance/spectral selectivity.

Keywords: borides; Ultra-High Temperature Ceramics; optical properties; solar absorbers; solar plants; concentrating solar power.

1. Introduction

Thanks to their ultra-refractory characteristics and their ability to withstand extreme and harsh environments, ultra-high temperature ceramics (UHTC) [1,2] based on boride, carbide and nitride materials are the best candidates for a variety of applications. Historically, their main application fields have been since a long time aerospace and military, as well as particularly demanding industrial contexts, e.g. thermonuclear reactors [3,4] and hypersonic applications [5-8]. Recently, we proved their intrinsic spectral selectivity and low thermal emittance and we proposed them as novel bulk solar absorbers for concentrating solar power (CSP), investigating different material parameters [9-20]. It should be noticed that CSP is considered one of the most promising renewable energy technologies [21], and, in addition, its efficiency increases with increasing operating temperature. Thus, the use of receiver materials able to sustain very high temperatures while maintaining good mechanical and thermal properties could generate a real innovation in this field.

Paper published on:
Solar Energy Materials and Solar Cells vol. 155 (2016), pages: 368–377
DOI: 10.1016/j.solmat.2016.06.028
http://www.sciencedirect.com/science/article/pii/S0927024816302033

To date, the research on CSP receivers has been mainly focused on silicon carbide (SiC) [22-23] and alumina (Al_2O_3) [24]. However, both these materials show serious drawbacks. SiC is a grey semiconductor with good solar absorbance and high oxidation resistance, but also high thermal emittance arising in large thermal losses at high temperature. On the other hand, Al_2O_3 is characterized by high refractoriness, high thermal stability and oxidation resistance, but, being white, also by very poor sunlight absorption properties. Thus, grey low-emissive and intrinsically spectrally selective UHTCs have a great potential for solar applications, once their properties would be carefully characterized and weaknesses addressed.

UHTCs are usually densified with the addition of sintering aids [25] to overcome problems related to the difficult strong covalent bonds of these refractory ceramics. One of the most suitable additives is $MoSi_2$. It has been found that a 10-15 vol% content of this phase is enough to enable full densification by either hot pressing or conventional sintering [26,27]. $MoSi_2$ has also proved to be effective in improving the oxidation resistance and high temperature strength of UHTCs [25].

The literature reports a large interest about studying the effect of different type and amount of sintering additives on borides. However, the main investigated characteristics are thermal [28-30] and mechanical properties [29,31], oxidation behavior [32,33] and porosity [29], while, to the best of our knowledge, the impact on optical properties remains unexplored. Thus, being them a key parameter for solar applications, similarly to the analysis we recently carried out on carbides [34], in this work we systematically investigate optical properties of $MoSi_2$-added zirconium, hafnium and tantalum diborides (ZrB_2, HfB_2 and TaB_2) as a function of the sintering aid amount or processing technique, correlating them to compositional and microstructural characteristics. For the three investigated borides, specimens with 10% and 20% $MoSi_2$ starting composition have been produced by hot pressing (HP) and pressureless (PS) sintering, respectively. In addition, fully dense ZrB_2-based composites containing $MoSi_2$ from 5 to 50 vol% were prepared in order to decouple process- from composition-related parameters and to study the effect of the secondary phase on the microstructural evolution, roughness, mechanical and optical properties.

2. Experimental

Commercial powders were used for the preparation of the materials listed in Tables I and II: hexagonal ZrB_2 (H. C. Starck, Germany. Grade B), mean particle size: 1.5 μm, impurities (wt%): C 0.25, O 2.0, N 0.25, Fe 0.1, Hf 0.2; hexagonal HfB_2 (Cerac Inc., Milwaukee, USA), mean particle size: 2.2 μm, impurities (wt%): Al 0.001, Fe 0.002, Zr<0.5; hexagonal TaB_2 (Materion Adv. Chemicals, Milwaukee, USA), mean particle size: 0.9 μm, impurities (wt%): Al 0.04, Cd<0.0007, Cr<0.0005, Fe 0.07, Nb 0.02, Pb<0.0004; tetragonal $MoSi_2$ (Aldrich, Milwaukee, USA), mean particle size: 2.8 μm, impurities (wt%): O 1.0. Samples to be sintered by hot pressing (HP) contained 10 vol% of $MoSi_2$, whilst those densified by pressureless sintering (PS) contained 20 vol% $MoSi_2$. Moreover a series of composites containing $MoSi_2$ from 5 to 50 vol% were prepared by hot pressing, as previously mentioned.

Matrix and additive were weighed in the proper amount and mixed through mechanical mixing for 24 h in absolute ethanol using SiC milling media. Subsequently the slurries were dried in a rotary evaporator and sieved through 250 μm screen. 30 to 45 mm-diameter pellets were green shaped by uniaxial pressing with 20 MPa.

The pellets to be sintered by hot pressing were directly placed in the furnace and hot pressed in low vacuum (~100 Pa) using an induction-heated graphite die with an uniaxial pressure of 30 MPa during the heating and a dwell at the maximum temperature set on the basis of the shrinkage curve, as reported in Tables I and II. On the other hand, the pellets to be sintered without applied pressure,

Paper published on:
Solar Energy Materials and Solar Cells vol. 155 (2016), pages: 368–377
DOI: 10.1016/j.solmat.2016.06.028
http://www.sciencedirect.com/science/article/pii/S0927024816302033

were preliminarily consolidated by cold isostatic pressing at 25 MPa and then sintered in a graphite furnace (Astro industries Inc., Santa Barbara, USA) with a heating rate of 600°C/h under flowing argon atmosphere (~0.1 MPa) in the temperature range 1750-1950°C, as indicated in Table I. All the composites cooled down naturally.

On the sintered materials, the bulk densities were measured by Archimedes' method and confirmed by SEM inspection. The relative density was thus estimated as the ratio between the measured value and the theoretical value determined through the rule of mixtures on the basis of starting nominal compositions.

The microstructure of the sintered ceramics was analysed on polished surfaces by scanning electron microscopy (FE-SEM, Carl Zeiss Sigma NTS Gmbh, Oberkochen, DE) and energy dispersive x-ray spectroscopy (EDS, INCA Energy 300, Oxford instruments, UK). Quantitative calculations of the microstructural parameters, like residual porosity, mean grain size and secondary phase content, were carried out via image analysis with a commercial software package (Image-Pro Plus® version 7, Media Cybernetics, Silver Springs, MD, USA).

The topological characterization of the surfaces was performed with a non-contact 3D profilometer (Taylor-Hobson CCI MP) on two areas of 0.08 x 1 cm^2 at the center of each sample and the topography data were analysed using a commercial software (Talymap 6.2). The evaluation of 2D texture parameters, like mean surface roughness (Ra) and distance between the highest asperity and the lowest valley (Rt), was performed on 4 different profiles (2 for each area) extracted from the 3D data and the gaussian filter (λc) for the separation of the roughness and waviness components was set according to the ISO 4288:2000. The 2D parameters were calculated as average of estimated values on all sampling lengths over each profile.

The room temperature flexural strength was measured according to the existing standard for advanced ceramics, method ENV 843-1, on chamfered bars with dimensions, 25 x 2.5 x 2.0 mm^3 (length by width by thickness, respectively), using a fully-articulated silicon carbide four-point fixture with a lower span of 20 mm and an upper span of 10 mm using a screw-driven load frame (Instron mod. 6025). The high temperature strength, up to 1770 K, was measured according to the ENV 820-1 standard. For the high-temperature tests, a soaking time of 18 min was set to reach thermal equilibrium. For each material, five samples were tested.

The hemispherical reflectance spectra were acquired using two instruments: a double-beam spectrophotometer (Lambda900 by Perkin Elmer) equipped with a Spectralon®-coated integration sphere for the 0.25-2.5 μm wavelength region and a Fourier Transform spectrophotometer (FT-IR "Excalibur" by Bio-Rad) equipped with a gold-coated integrating sphere and a liquid nitrogen-cooled detector for the range 2.5-16.5 μm.

Label	Matrix	$MoSi_2$ vol%	Sintering	T,t,P °C,min,MPa	Final ρ g/cm^3	Rel. ρ %	Pores %	m.g.s. μm	Min g.s. μm	Max g.s. μm	Secondary phases by SEM-EDS vol%
Z10HP	ZrB_2	10	HP	1850,10,20	6.1	98.3	3.7	2.4±0.6	1.4	3.9	8.5 $MoSi_2$, 1.4 SiO_2, 0.7 SiC
Z20PS		20	PS	1950,60,-	6.1	99.0	0.8	2.6±0.7	1.3	4.1	18 $MoSi_2$, 2 MoB, 0.5 SiO_2
H10HP	HfB_2	10	HP	1900,8,30	10.1	96.4	0	0.8±0.3	0.3	2.3	5 $MoSi_2$, 3 HfO_2, 2 SiO_2
H20PS		20	PS	1950,60,-	10.0	98.0	1.4	1.4±0.8	0.4	4.9	15 $MoSi_2$, 2 Mo_5Si_3,

Paper published on:
Solar Energy Materials and Solar Cells vol. 155 (2016), pages: 368–377
DOI: 10.1016/j.solmat.2016.06.028
http://www.sciencedirect.com/science/article/pii/S0927024816302033

											0.5 HfO_2
T10HP	TaB_2	10	HP	1690,10,30-40	10.2	95.4	1.3	3.8±1.1	1.7	6.7	3 $MoSi_2$, 9 SiO_2/SiC
T20PS		20	PS	2100,180,-	9.2	(90.4) 97.0	3.0	38.4±13.6	13.6	84.2	10 $MoSi_2$, 8 Si, 4 SiC

PS: pressureless sintering
HP: hot pressing

Table I: *Composition, sintering parameters (T: maximum temperature, t: dwell at T, P: applied pressure), final and relative densities (ρ), mean grain size (m.g.s.), smallest (Min g.s.) and largest (Max g.s.) grain size and secondary phases of the borides sintered with $MoSi_2$. Porosity is estimated by image analysis.*

Label	Matrix	$MoSi_2$ vol%	T,t,P °C,min,MPa	Final ρ g/cm³	Rel. ρ %	Porosity %	m.g.s. µm	Max g.s. µm	Min g.s. µm	Secondary phases by SEM-EDS vol%
Z5HP	ZrB_2	**5**	1900,10,30	5.96	97.5	0.2	1.9±0.7	3.6	0.9	1.4 $MoSi_2$, 1.5 SiO_2/SiC
Z10HP		10	1850,10,30	6.1	98.3	3.7	2.4±0.6	3.9	1.4	8.5 $MoSi_2$, 1.4 SiO_2, 0.7 SiC
Z20HP		20	1800,4,30	5.89	95.8	0.1	2.4±0.9	5.4	0.6	13 $MoSi_2$, 2.5 SiO_2, 2.0 SiC, 0.7 $ZrO_2$2, 0. MoB
Z30HP		30	1850,3,30	5.95	96.5	0.2	1.7±0.6	3.6	0.6	28.4 $MoSi_2$, 3.4 SiO_2/SiC
Z50HP		50	1750,13,30	5.89	94.9	0.3	1.9±0.8	4.3	0.7	39 $MoSi_2$, 6.5 SiO_2, 2 MoB, 1 ZrO_2, 1 SiC

Table II: *Composition, sintering parameters (T: maximum temperature, t: dwell at T, P: applied pressure), final and relative densities (ρ), mean, maximum and minimum grain size (m.g.s.) and secondary phases of the ZrB_2-based composites sintered by hot pressing with increasing amount of $MoSi_2$. Porosity is estimated by image analysis.*

3. Results

3.1 Microstructural features

To correlate optical spectra to compositional characteristics, SEM image analysis was carried out on the optically investigated surfaces.

HP ZrB_2- 10 $MoSi_2$ – The Z10HP ceramic started to shrink at around 1500°C and reached a density of 6.1 g/cm³ after holding 1750°C for 20 minutes (Table I). Microstructural analysis carried out on the optical surface revealed however a porosity level between 3-4%, probably due to partial grains removal during polishing procedure. In Fig. 1a, ZrB_2 exhibits rounded grains with mean grain size around 2.4 µm, while $MoSi_2$ is characterized by an irregular shape with low dihedral angles. Silica pockets with nitrogen impurities were recognizable as dark contrasting phases and often contained small SiC grains, deriving from its carbo-reduction in the furnace environment. The amount of silica and SiC was estimated to be below 2 vol% by image analysis. Small amounts of ZrO_2, ZrC, and a Zr-C-O phase were also detected. Below Fig. 1a a detailed view of the matrix grains is shown. ZrB_2 grains have a core-shell substructure. The core is constituted by original ZrB_2 grains and the shell by a $(Zr,Mo)B_2$ solid solution, with an amount of Mo around 5 at%, which grew epitaxially on the core [26].

The microstructural features relative to the hot pressed ZrB_2 composites with various $MoSi_2$ content (5, 20, 30, 50) are analogous to what has been just illustrated for Z10HP. Examples of the optical surfaces of samples containing 5, 20, 30 and 50 vol% $MoSi_2$ are shown in Fig. 2, with

Paper published on:
Solar Energy Materials and Solar Cells vol. 155 (2016), pages: 368–377
DOI: 10.1016/j.solmat.2016.06.028
http://www.sciencedirect.com/science/article/pii/S0927024816302033

detailed description in Table II. The mean grain size of these ZrB_2-based composites was not statistically different varying the $MoSi_2$, as well as the minimum and maximum grains dimension. One thing that has to be noticed is that the final effective $MoSi_2$ content was slightly different from the nominal one, partially due to its dissociation into Mo and Si, that entered in the $(Zr,Mo)B_2$ solid solution and formed SiO_2/SiC, respectively, [26] and partially due to pullout occurred during polishing procedure.

PS ZrB_2- 20 $MoSi_2$ – The Z20PS ceramics achieved the full density after sintering in graphite furnace at 1950°C for 60 minutes. Image analysis confirmed a porosity level below 1%. The polished section of the optical surface displayed in Fig. 1b shows rounded ZrB_2 grains with grain size similar to the material sintered by hot pressing, 2.6 µm, and with the same core-shell sub-structure. The $MoSi_2$ phase is characterized by irregular shape and bright contrast. In addition, about 2 vol% of MoB and Mo_5Si_3 are often found adjacent to $MoSi_2$. Occasionally, SiO_2 pockets were detected in the microstructure.

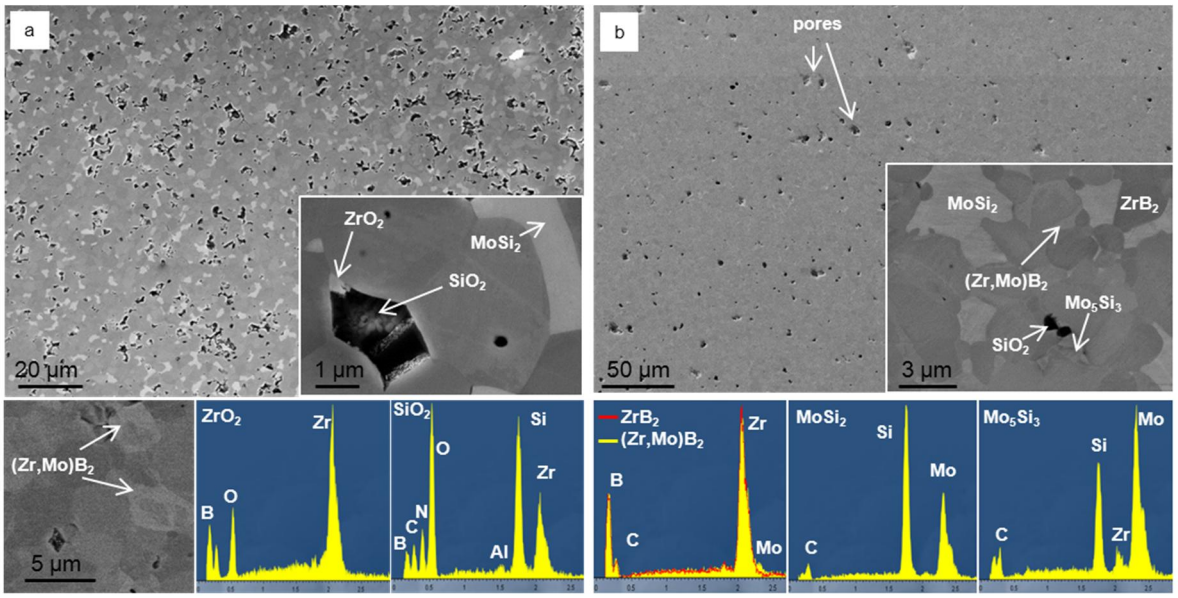

Figure 1: *SEM images of the microstructure of ZrB_2-based composites sintered by a) hot pressing and 10 vol% of $MoSi_2$ (Z10HP) and b) pressureless sintering and 20 vol% of $MoSi_2$ (Z20PS).*

Paper published on:
Solar Energy Materials and Solar Cells vol. 155 (2016), pages: 368–377
DOI: 10.1016/j.solmat.2016.06.028
http://www.sciencedirect.com/science/article/pii/S0927024816302033

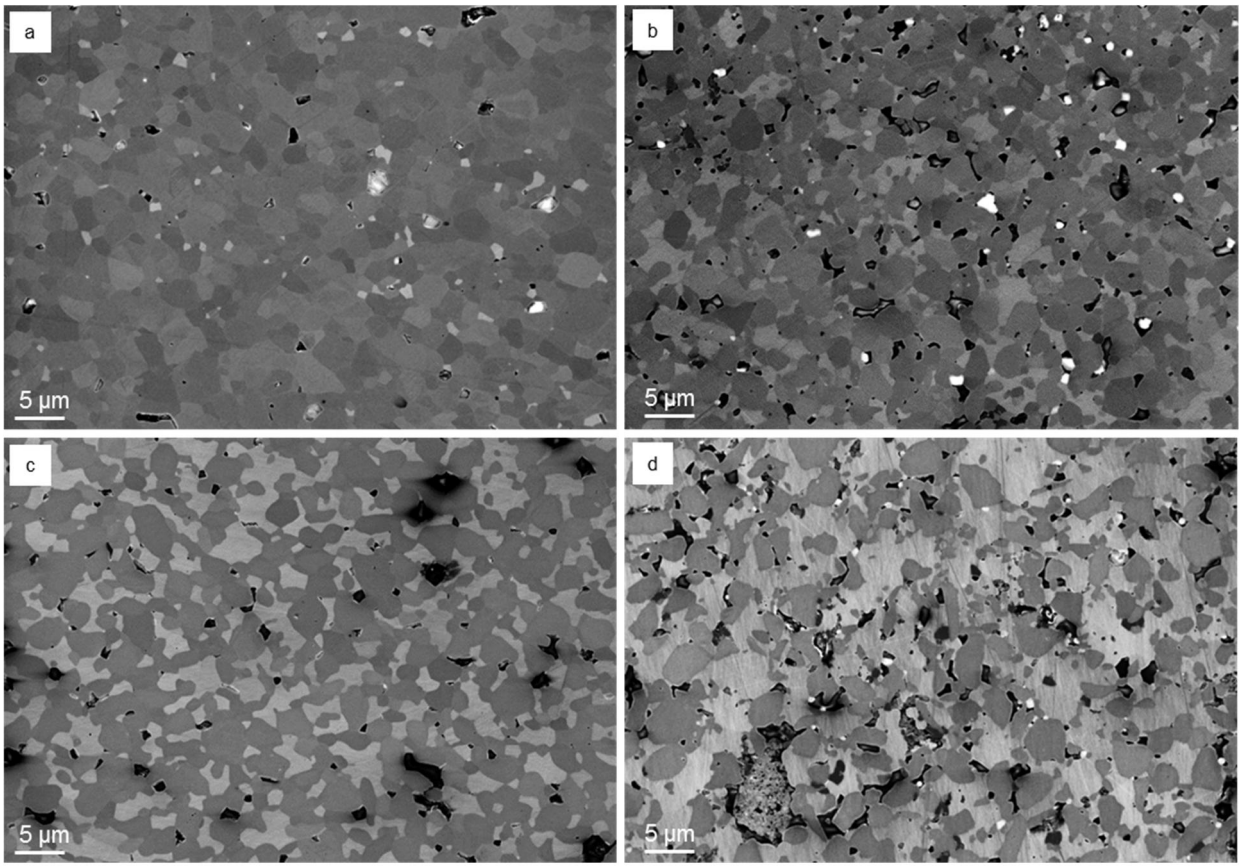

Figure 2: *SEM images of the microstructure of ZrB_2-based composites sintered by hot pressing and containing a) 5, b) 20, c) 30 and d) 50 vol% of $MoSi_2$.*

HP HfB_2- 10 $MoSi_2$ - Being HfB_2 highly refractory, the temperature at which H10HP composite started to shrink was above 1800°C, and 1900°C were necessary to complete the densification. In Fig. 3a, a polished section reveals a homogeneous microstructure with little residual porosity and without macrodefects. HfB_2 grains have a rounded shape with mean grain size about 1.0 µm, while the $MoSi_2$ phase has an irregular morphology with concave shapes and dark contrast. Its amount is reduced from 10 to 5 vol%, owing to its dissociation into SiO_2, found in the microstructure, and Mo, which entered the HfB_2 lattice, originating a $(Hf,Mo)B_2$ solid solution around a HfB_2 core, likewise ZrB_2-system, [26] inset in Fig. 3a. In analogy to the ZrB_2-$MoSi_2$ system, the analysis of secondary phases by EDS confirmed the presence of HfO_2, which appears as rounded bright particles, HfC and Hf-B-C-O spurious phases.

PS HfB_2- 20 $MoSi_2$ – Sintering at 1950°C resulted in a final density of H20PS around 98% of the theoretical density and image analysis confirmed a residual porosity around 1.4%. In Fig. 3b, the polished section shows a very regular microstructure, with little residual porosity. HfB_2 grains have a rounded shape with mean grain size of about 1.5 µm while the $MoSi_2$ phase has an irregular morphology and its amount is reduced from 20 to 15 vol%, like for the previous materials. Also in this case, a $(Hf,Mo)B_2$ solid solution formed, with Mo content in the order of 5 at%. The analysis of secondary phases by EDS confirmed the presence of Mo_5Si_3, darker than $MoSi_2$, and HfO_2, which appears as bright round particles, inset in Fig. 3b.

Paper published on:
Solar Energy Materials and Solar Cells vol. 155 (2016), pages: 368–377
DOI: 10.1016/j.solmat.2016.06.028
http://www.sciencedirect.com/science/article/pii/S0927024816302033

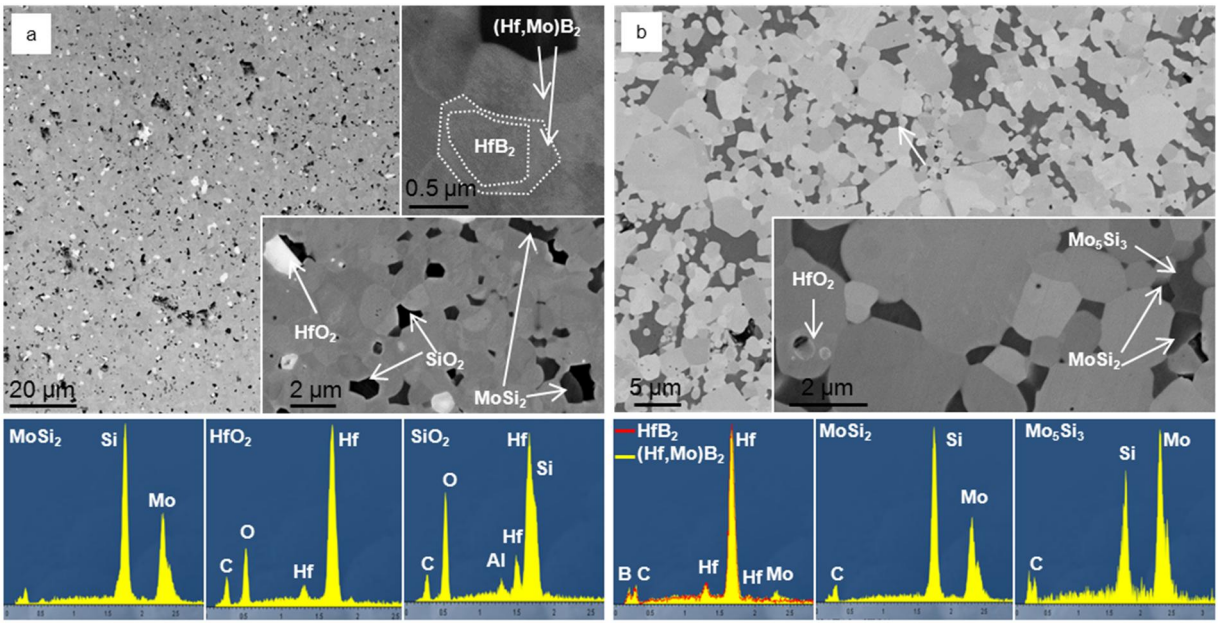

Figure 3: *SEM images of the microstructure of HfB_2-based composites sintered by a) hot pressing and 10 vol% of $MoSi_2$ (H10HP) and b) pressureless sintering and 20 vol% of $MoSi_2$ (H20PS).*

HP TaB_2- 10 $MoSi_2$ - The T10HP composite started to shrink at 1530°C, but at 1680°C no further movement of the rams was measured. Despite being sintered at the lowest temperature among the UHTCs just presented, this composite had a dense microstructure, with residual porosity in the order of 1-2%, and good adhesion was found between matrix and secondary phase. The polished surface showed a multi-phase microstructure (Fig. 4a), the bright phase with mean grain size around 3-4 µm is a $(Ta,Mo)B_2$, solid solution with about 5 at% of Mo. The grey phase is $MoSi_2$, found on the surface in very little amount, about 3 vol%, whilst the dark phases are SiO_2 and Si-O-C, in amount around 8 vol%. The presence of high amount of SiO_2 in the final microstructure is related to the low sintering temperature, 1680°C, compared to other Zr- and Hf-borides, sintered at 1750 and 1900°C respectively, temperatures at which carbo-reduction is strongly favorable. Indeed, inside SiO_2 droplets, SiC nano-crystals can be often found, as the example in the inset of Fig. 4a. At the triple junctions, dark regions containing Ta-Si-B-O and Ta-Si-C-O were observed and intergranular films could also be noticed [35].

PS TaB_2- 20 $MoSi_2$ – The T20PS composite was sintered at 2100°C with a $MoSi_2$/BN powder bed to limit $MoSi_2$ dissociation. The final density resulted equal to 9.2 g/cm^3. Like for T10HP this value could be underestimated owing to the formation of low density phases, which decreased the theoretical density. A SEM image of T20PS is displayed in Fig. 4b and shows that TaB_2 has a squared shape and its mean grain size notably increased during sintering passing from 5-10 µm of the starting powder to an average of 38 µm, with grains up to 84 µm. EDS carried out on the matrix grains, revealed about 10 at% of Mo inside the boride, resulting in a $(Ta_{0.9}Mo_{0.1})B_2$ solid solution. Residual $MoSi_2$, around 10 vol%, has grey contrast and irregular shape filling the space among TaB_2 grains. Adjacent to the sintering additive other two phases with the same shape but darker contrast can be seen, inset in Fig. 4b. EDS analyses revealed to be about 4 vol% of SiC and 8 vol% of Si. The formation of these new species is due to the high sintering temperature and C-rich

Paper published on:
Solar Energy Materials and Solar Cells vol. 155 (2016), pages: 368–377
DOI: 10.1016/j.solmat.2016.06.028
http://www.sciencedirect.com/science/article/pii/S0927024816302033

atmosphere favoring $MoSi_2$ dissociation. Both SiC, Si and $MoSi_2$ seem to be very reactive to the matrix grains at the sintering temperature, as TaB_2 grains are also featured by corroded edges. About 3% of rounded porosity was also present, especially inside $MoSi_2$ phase, probably owing to its low viscosity at the sintering temperature. This porosity well matches with the recalculate theoretical density including the newly formed phase, 97%.

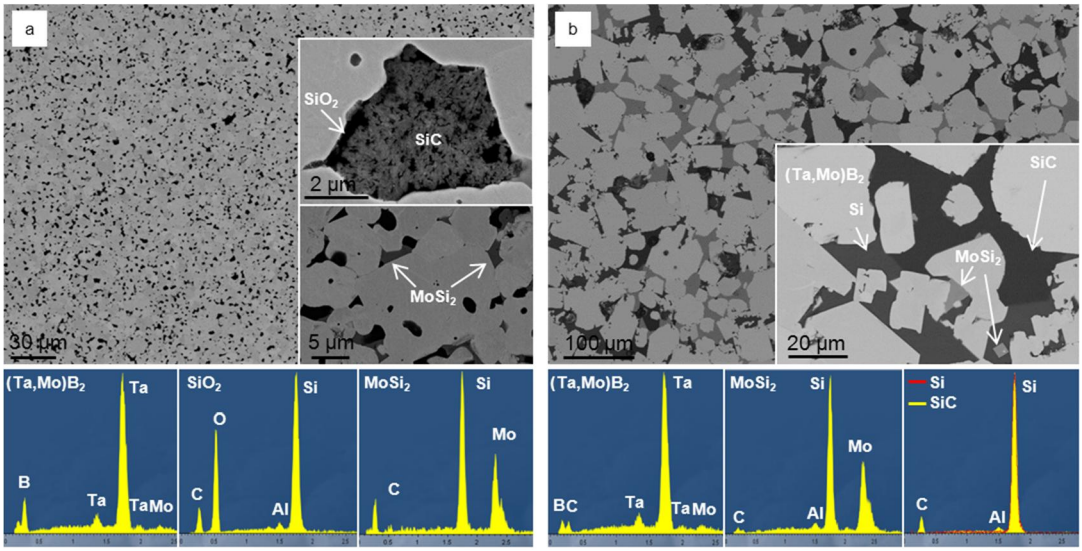

Figure 4: *SEM images of the microstructure of TaB_2-based composites sintered by a) hot pressing and 10 vol% of $MoSi_2$ (T10HP) and b) pressureless sintering and 20 vol% of $MoSi_2$ (T2PS).*

3.2 Roughness measurements

The topological characterization of the optical surfaces revealed that average roughness, Ra, and maximum distance between peak and valley, Rt, for the composites densified by hot pressing and pressureless follow the same trend, therefore, for simplicity, only Ra will be discussed, Fig. 5. The overall trend observed for analogous materials [34] is confirmed, i.e. Ra increases either with increasing porosity or larger mean grain size.

Specifically, hot pressed materials generally achieved smoother surfaces than the corresponding composites sintered without pressure, owing to a higher relative density and smaller mean grain size, Fig. 5a. The only exception is for Z10HP which results slightly rougher than Z20PS, with Ra=25 and 11 nm, respectively, due to the higher surface porosity of the first sample. Similar Ra values are measured for HfB_2-composites, in view of close microstructural features. On the other hand, T20PS, densified by pressureless sintering, shows a roughness more than four times that of T10HP densified by hot pressing, owing to the notably coarser microstructure, ten times bigger, Table I.

As far as the amount of the secondary phase is concerned, Fig. 5b shows the plot of the average roughness for the hot pressed composites containing 5-50 vol% of $MoSi_2$. The plot clearly shows an asymptotic dependence of the surface roughness with the content of secondary phase, which tends to be stable from 20 vol% on. This trend does not seem to clearly match with none of the parameters supposed to affect the roughness, like surface porosity or mean grain size.

Paper published on:
Solar Energy Materials and Solar Cells vol. 155 (2016), pages: 368–377
DOI: 10.1016/j.solmat.2016.06.028
http://www.sciencedirect.com/science/article/pii/S0927024816302033

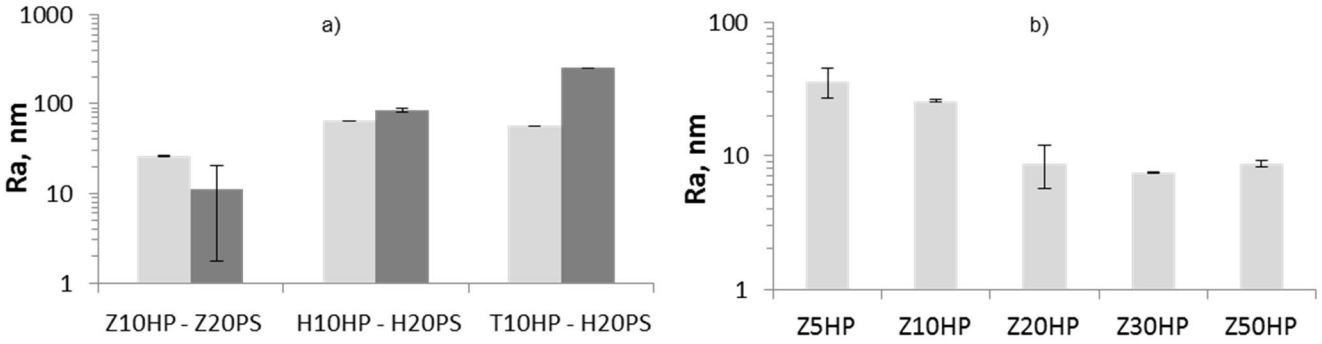

Figure 5: *Plots of the average roughness, Ra, measured on the optical surface of a) the borides sintered by hot pressing or pressureless sintering and b) ZrB_2 sintered by hot pressing and containing increasing amount of $MoSi_2$.*

3.3 Mechanical properties

The four-point flexural strength of the borides at room temperature and at 1770 K is reported in Fig. 6, the mechanical properties of sintered in graphite furnace, T20PS, were not measured owing to the coarse microstructure certainly leading to poor strength.

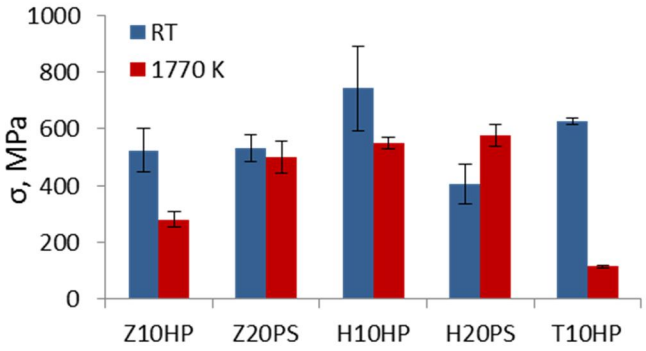

Figure 6: *Plots of 4-points flexural strength of borides at room or at high temperature as a function of the sintering technique.*

The room temperature strength of Z10HP and Z20PS composites is statistically not different, but at 1770 K differences emerge, Fig. 6. The strength of ZrB_2 obtained by hot pressing collapses from 524 to 280 MPa, probably due to residual silica softening (see Tab. I), on the other hand, ZrB_2 obtained by pressureless sintering maintains its strength, thanks to the higher sintering temperature which favored the elimination of residual Si-O based phases. As for HfB_2-based materials, the presence of higher amount of $MoSi_2$ induces a strength decrease from about 740 MPa for H10HP to 400 MPa for H20PS at room temperature. It has been noticed indeed, that $MoSi_2$ tends to form 20-60 μm agglomerates during processing that act as critical flaws during room temperature fracture [27, 36]. A better dispersion of this secondary phase could limit this strength drop. For this system, the same trend observed for ZrB_2-based ceramics is found passing from room to high temperature, i.e. strength retention or even increase. In the case of TaB_2 processed by hot pressing, the room temperature strength falls in the range of the other borides, around 630 MPa, but at high

Paper published on:
Solar Energy Materials and Solar Cells vol. 155 (2016), pages: 368–377
DOI: 10.1016/j.solmat.2016.06.028
http://www.sciencedirect.com/science/article/pii/S0927024816302033

temperature the notable presence of SiO_2 provokes a strength reduction of 80% of the room temperature value.

These results indicate that the borides at hand have a great potential in terms of strength and refractoriness, but the content of softening phases, like SiO_2, needs to be kept as low as possible, as it is responsible for strength drop already in amount as small as 2 vol% (Z10HP), and is deleterious in amount of 9 vol% (T10HP).

3.4 Optical characterization

Figure 7 compares the hemispherical reflectance spectra of the different materials as a function of the sintering technique.

For ZrB_2, Fig. 7a, the two investigated samples have very similar spectra, with absolute reflectance differences lower than 3%. Z10HP has a slightly higher reflectance than Z20PS in the infrared above 2 μm, while the reflectance value of Z20PS is the highest at shorter wavelengths. Also in the case of HfB_2, Fig. 7b, the samples show similar curves. The largest difference among them lies in the region about 2.8 μm (about 10% difference in hemispherical reflectance), where H20PS shows a minimum due to higher amount of residual $MoSi_2$, as it can be easily recognized by comparing the boride spectra to that of a reference $MoSi_2$ specimen.

As for spectral signatures of secondary phases, we should notice that $MoSi_2$ itself shows SiO_2 impurities. If we compare the spectrum of $MoSi_2/SiO_2$ with that of pure SiO_2, we can tentatively assign to SiO_2 secondary phase the small feature in the $MoSi_2$ spectrum at around 9 μm (Figure 8). As we will detail in the following, this attribution allows fairly well explaining the spectra of borides.

If we consider tantalum boride (Fig. 7c), the two samples show larger differences among them, likely due to the considerable difference in their roughness values (57 vs 257 μm Ra for T10HP and T20PS, respectively). If we compare the acquired curves for borides and pure $MoSi_2$, for TaB_2 we can clearly identify in both T10HP and T20PS the spectral feature revealing $MoSi_2$ (the small slope change at around 2.8 μm, likely connected to the minimum in the $MoSi_2$ spectrum). The shoulder at around 9 μm in T10HP, which appears to be more pronounced than the $MoSi_2$ dip at 2.8 μm and is absent in T20PS, can thus be ascribed to SiO_2 rather than to the silicide, as compositional analysis discloses the oxide in T10HP (9 vol% SiO_2, Table I). Coherently to microstructural analysis, SiO_2 peak is not shown in the spectrum of T20PS. On the other hand, for pressureless sintered TaB_2 (T20PS), which, according to microstructural analysis, has a higher $MoSi_2$ content than the corresponding HP specimen (10 vs 3 vol%), the spectral signature of $MoSi_2$ is more pronounced. Spectral signals coming from other secondary phases like SiC, which should be recognized by a feature at around 12 μm [37], cannot be detected. This could be likely due to the notably higher roughness of this sample, arising in a lower overall reflectance hiding small spectral features.

(a)

Paper published on:
Solar Energy Materials and Solar Cells vol. 155 (2016), pages: 368–377
DOI: 10.1016/j.solmat.2016.06.028
http://www.sciencedirect.com/science/article/pii/S0927024816302033

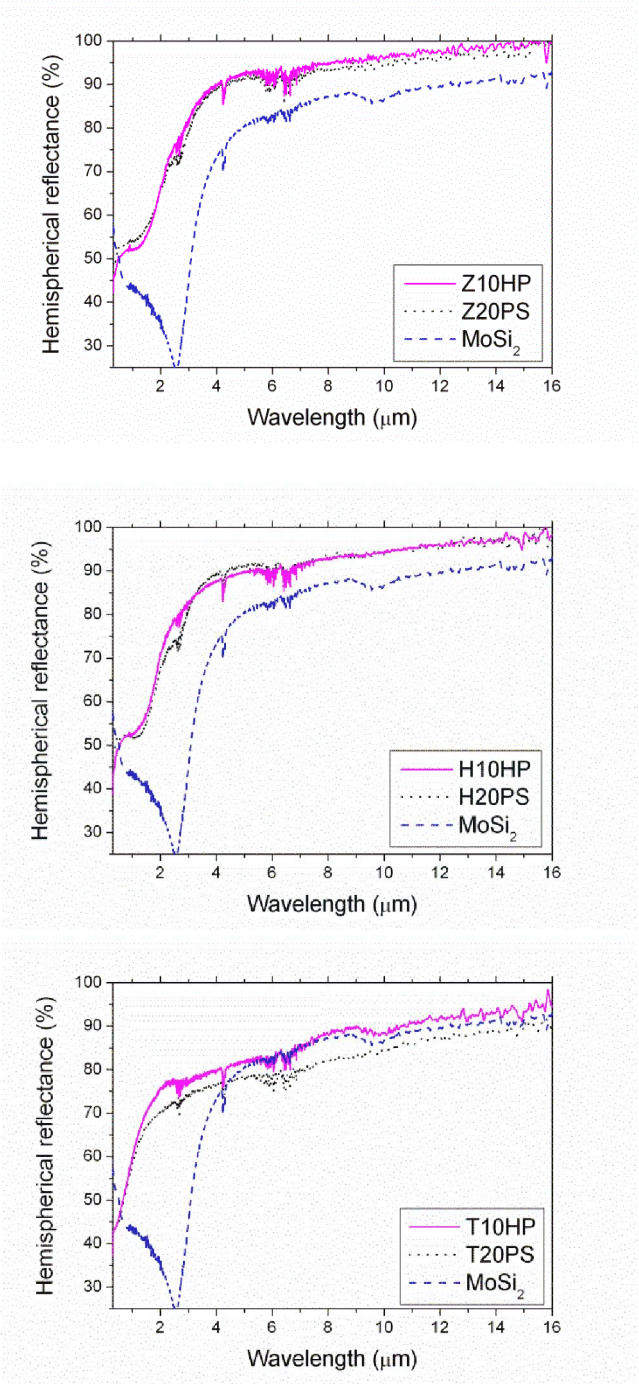

(b)

(c)

Figure 7: *Comparison of hemispherical reflectance spectra of different borides as a function of the additive amount. The spectrum of $MoSi_2$ is also shown for reference.*

Paper published on:
Solar Energy Materials and Solar Cells vol. 155 (2016), pages: 368–377
DOI: 10.1016/j.solmat.2016.06.028
http://www.sciencedirect.com/science/article/pii/S0927024816302033

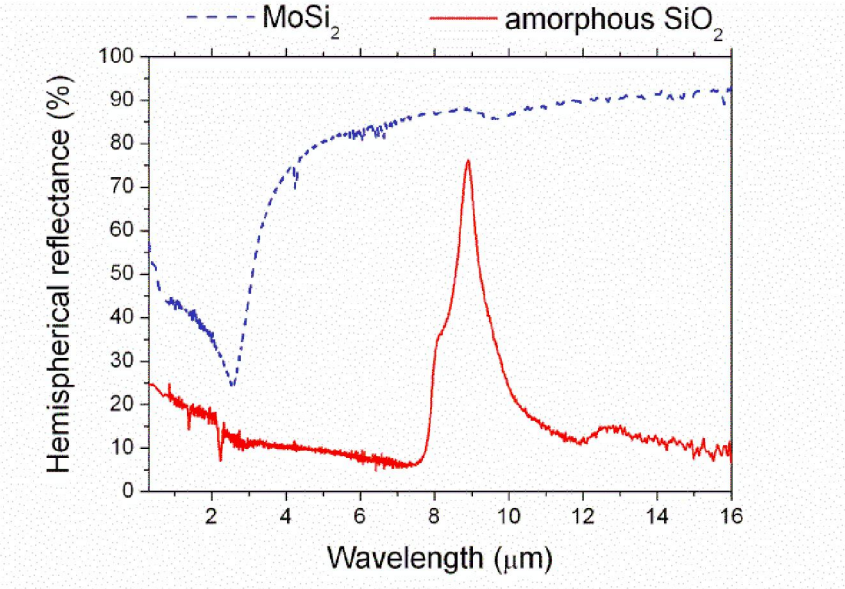

***Figure 8**: MoSi₂ and SiO₂ reflectance spectra*

Figure 9 compares the spectra of the different materials for fixed processing technique, i.e. for fixed $MoSi_2$ amount. We can appreciate that the spectral shapes of ZrB_2 and HfB_2 curves are very similar and TaB_2 always has the lowest reflectance for wavelengths longer than about 2 μm and shorter than about 1 μm, while in the intermediate region 1-2 μm its reflectance is by far the highest. The feature at around 9 μm can be clearly identified only in hot pressed TaB_2 (T10HP), in agreement with its much higher SiO_2 content than other hot pressed materials. As for HfB_2 and ZrB_2, the more pronounced shoulder at around 2.8 μm of PS samples with respect to HP specimens agrees with their higher $MoSi_2$ content, see Table I.

Paper published on:
Solar Energy Materials and Solar Cells vol. 155 (2016), pages: 368–377
DOI: 10.1016/j.solmat.2016.06.028
http://www.sciencedirect.com/science/article/pii/S0927024816302033

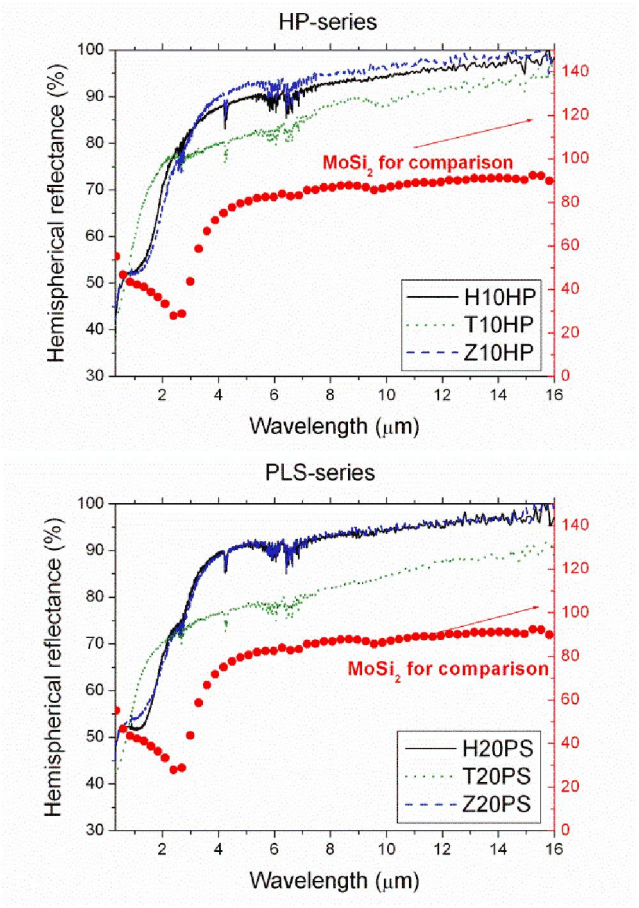

Figure 9: *Comparison of hemispherical reflectance spectra of different borides for fixed sintering aid content. The spectrum of $MoSi_2$ is also shown for reference and referred to a different scale (right axis, where physically meaningless labels higher than 100% are shown only for visualization purposes).*

Figure 10a shows the spectra of the various hot pressed ZrB_2 samples as a function of the sintering aid amount, ranging from 5 to 50 vol% in the nominal composition. In the sample with the lowest $MoSi_2$ amount, no $MoSi_2$ or SiO_2 signals are detected, in agreement with the very low content proved by microstructural analysis. As the original composition is enriched in $MoSi_2$, $MoSi_2$ signature starts to appear in the spectra and progressively increases proportionally. Similarly, the peak attributed to SiO_2 increases in intensity, in agreement with the increasing of SiO_2 phase content from Z20HP to Z50HP. It is interesting to notice (Figure 10b***)*** that the reflectance curve of Z50HP can be fairly reproduced by a linear combination of almost pure ZrB_2 (Z5HP) and reference $MoSi_2$ (with SiO_2 impurities) in a rough 1:1 ratio.

Paper published on:
Solar Energy Materials and Solar Cells vol. 155 (2016), pages: 368–377
DOI: 10.1016/j.solmat.2016.06.028
http://www.sciencedirect.com/science/article/pii/S0927024816302033

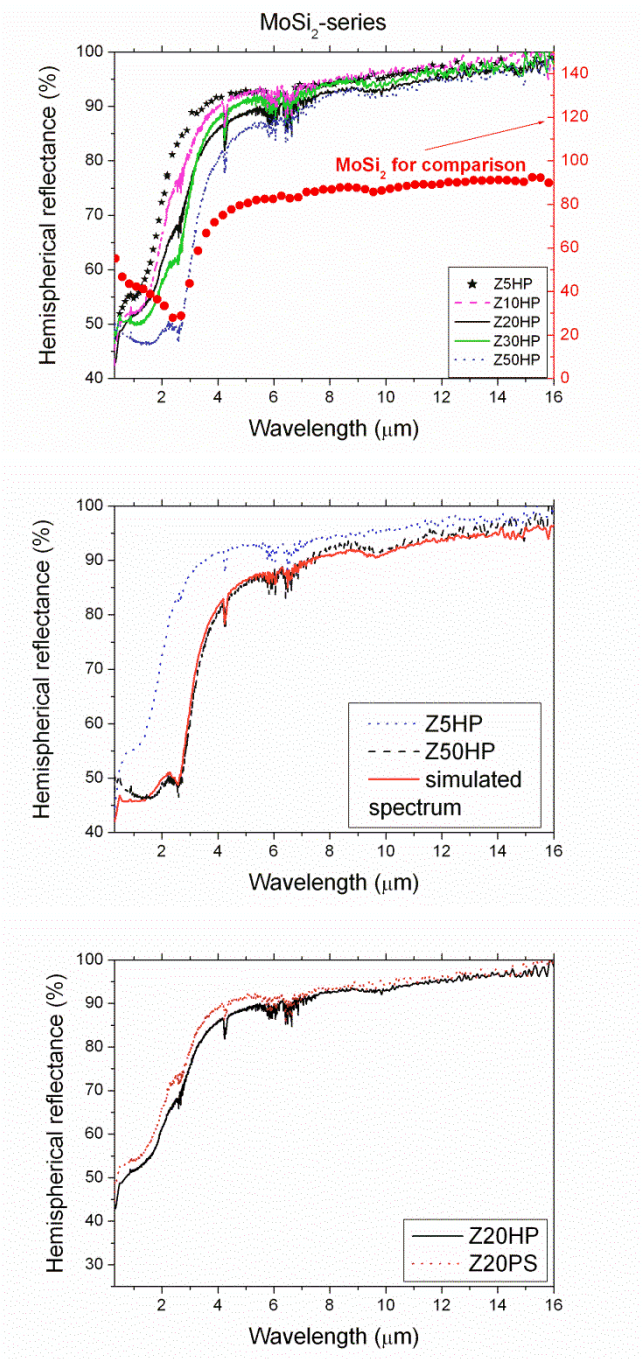

Figure 10: *a) Hemispherical reflectance spectra of hot pressed ZrB_2 as a function of increasing $MoSi_2$ content. b) Tentative simulation of the spectrum of sample Z50HP, demonstrating the impact of $MoSi_2$ on its surface. c) Spectra of ZrB_2 samples containing 20 vol% of $MoSi_2$ produced with different processing techniques.*

Finally in Figure 10c we show the spectra of two ZrB_2 samples with the same nominal composition, but produced with different techniques. We can appreciate that both curves show the $MoSi_2$ dip and that the sample produced by the HP technique (Z20HP) is characterized by a lower reflectance in the whole spectral region. For wavelengths shorter than 6 μm, the two curves are

Paper published on:
Solar Energy Materials and Solar Cells vol. 155 (2016), pages: 368–377
DOI: 10.1016/j.solmat.2016.06.028
http://www.sciencedirect.com/science/article/pii/S0927024816302033

roughly parallel. This behavior cannot be explained neither by the different roughness, as the sample with the (even slightly) higher roughness also shows the highest reflectance, neither by the different $MoSi_2$ content, as the impact of the $MoSi_2$ dip on the spectra is similar and, again, the sample containing a higher amount of $MoSi_2$ (18% vs 13%) shows the highest reflectance, neither, finally, by different grain size, because grain sizes are also similar. The parameter most significantly changing from Z20PS and Z20HP samples is the SiO_2 content (0.5% vs 2.5%) and allows to explain the experimental curves. In fact, the reflectance is lower in the sample containing a larger amount of SiO_2, because SiO_2 (whose shoulder at 9 μm can be clearly recognized in Z20HP) is characterized by very low reflectance values in spectral regions outside its vibrational peaks (Figure 8).

From the experimental room-temperature hemispherical reflectance $\rho^{\frown}(\lambda)$ we calculated the total solar absorbance, α:

$$\alpha = \frac{\int_{\lambda_{min}}^{\lambda_{max}} (1-\rho^{\frown}(\lambda)) \cdot S(\lambda) d\lambda}{\int_{\lambda_{min}}^{\lambda_{max}} S(\lambda) d\lambda} \qquad (1)$$

where S(λ) is the Sun emission spectrum [38] and the integration is carried out between λ_{min}=0.3 μm and λ_{max}=3.0 μm; and an estimated hemispherical emittance, ε, at 1200 K:

$$\varepsilon = \frac{\int_{\lambda 1}^{\lambda 2} (1-\rho^{\frown}(\lambda)) \cdot B(\lambda,1200K) d\lambda}{\int_{\lambda 1}^{\lambda 2} B(\lambda,1200K) d\lambda} \qquad (2)$$

where B(λ,1200K) is the blackbody spectral radiance at 1200K temperature and λ1=0.3 μm and λ2=16.0 μm. The α/ε ratio (sometimes called spectral selectivity) is a parameter assessing the material potential for solar receiver applications, and ideally should be taken as high as possible. Figure 11 compares the calculated α/ε ratios as a function of processing technique. The variability range for α/ε lies between 1.9 and 2.6. For a given material, HP samples (10 vol% $MoSi_2$) always show a slightly higher α/ε value than PS ones (20 vol% $MoSi_2$). ZrB_2 and HfB_2 are similarly performing, while α/ε ratios for TaB_2 are generally lower. However, as process and $MoSi_2$ amount (i.e. secondary phases in the final product) are coupled parameters in these samples, Figure 12 shows the calculated α/ε values for hot pressed ZrB_2 as a function of the nominal $MoSi_2$ content to clarify which parameter more significantly impacts on optical performances. The trend in Figure 12 is immediately evident, suggesting that, at least for the investigated boride matrix, the worsening of spectral selectivity can be ascribed to the increasing content of $MoSi_2$ and related secondary phases.

Paper published on:
Solar Energy Materials and Solar Cells vol. 155 (2016), pages: 368–377
DOI: 10.1016/j.solmat.2016.06.028
http://www.sciencedirect.com/science/article/pii/S0927024816302033

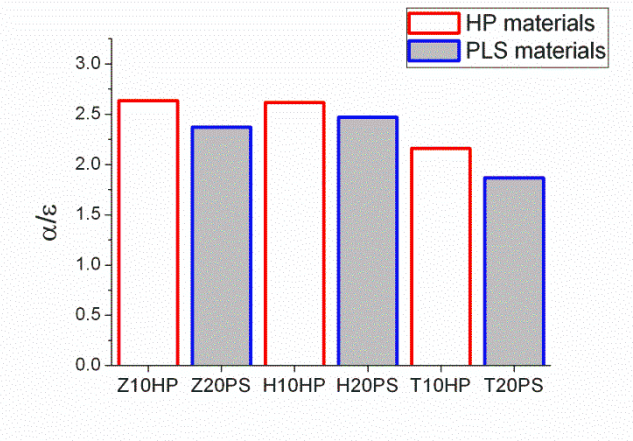

Figure 11: *Calculated α/ε ratios for materials produced with different processing techniques.*

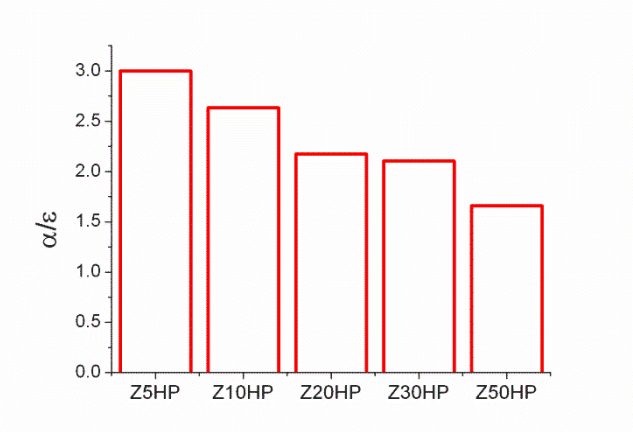

Figure 12: *Calculated α/ε ratios for hot pressed ZrB_2 samples.*

As a final comment, it should be mentioned that investigated borides (α≈0.5) and UHTCs in general are typically characterized by absorbance values lower than those of silicon carbide, even if significantly higher than those of white absorbers e.g. alumina [34]. However, it has been recently demonstrated, for the case of hafnium carbide [18] that solar absorbance can be significantly increased by proper surface treatments.

Conclusions

In this work we systematically investigated and compared ZrB_2, HfB_2 and TaB_2 produced by both high pressure and pressureless sintering techniques and corresponding to the use of 10 and 20 vol% of $MoSi_2$ sintering aid, respectively. Moreover, for ZrB_2 produced through high pressure method, we studied the effect of the $MoSi_2$ nominal content, ranging from 5 to 50 vol%, on the microstructural evolution, roughness, mechanical and optical properties.

PS specimens typically display larger grain size, rougher surface, lower fracture strength and slightly worse optical performances (lower α/ε ratio) than the corresponding HP samples, but the high temperature strength is generally better, thanks to elimination of residual SiO_2 in the as-sintered microstructure

Paper published on:
Solar Energy Materials and Solar Cells vol. 155 (2016), pages: 368–377
DOI: 10.1016/j.solmat.2016.06.028
http://www.sciencedirect.com/science/article/pii/S0927024816302033

For the HP ZrB_2 series, increasing $MoSi_2$ amount poorer mechanical and optical performances are connected to the SiO_2, which always accompanies the silicide .

Thus, for future solar absorber applications, the addition of $MoSi_2$ sintering aid should be not higher than 10 vol% in order to ensure good sinterability and oxidation protection at high temperature. As for the comparison among different matrices, for fixed processing technique HfB_2 and ZrB_2 show similar spectra, while the lower infrared reflectance of TaB_2 arises in a lower α/ε ratio, remaining however higher than that of the reference SiC ($\alpha/\varepsilon=1$).

Acknowledgements

Part of this activity has been carried out in the framework of the FIRB2012-SUPERSOLAR project funded by the Italian Ministry of University and Research (Programma “Futuro in Ricerca”, prot. RBFR12TIT1). E. S. gratefully acknowledges the Italian bank foundation “Fondazione Ente Cassa di Risparmio di Firenze” for providing the grant for M.M. within the framework of the “SOLE” and “SOLE-2” projects (pratiche n. 2013.0726 and 2014.0711). Thanks are due to Mr. M. D’Uva and Mr. M. Pucci (CNR-INO) for technical assistance.

References

[1] W. G. Fahrenholtz, E. J. Wuchina, W. E. Lee, Y. Zhou eds., Ultra-High Temperature Ceramics: Materials for Extreme Environment Applications, (Wiley, 2014)

[2] E. Wuchina, E. Opila, M. Opeka, W. Fahrenholtz, I. Talmy, UHTCs: Ultra-High Temperature Ceramic Materials for Extreme Enviroment Application, The Electrochemical Society Interface (2007) 30–36

[3] W. E. Lee, M. Gilbert, S. T. Murphy, R. W. Grimes, Opportunities for Advanced Ceramics and Composites in the Nuclear Sector, J. American Ceramic Society 96 (2013) 2005-2030

[4] W. E. Lee, E. Giorgi, R. Harrison, A. Maître, O. Rapaud, Nuclear Applications for Ultra-High Temperature Ceramics and MAX Phases, in: Ultra-high temperature ceramics: materials for extreme environment applications, edited by William G. Fahrenholtz, Eric. J. Wuchina, William E. Lee, Yanchun Zhou (Wiley 2014)

[5] T. H. Squire, J. Marschall, Material property requirements for analysis and design of UHTC components in hypersonic applications, J. European Ceramic Society 30 (2010) 2239–2251

[6] R. Loehman, E. Corral, H. P. Dumm, P. Kotula, R. Tandon, Ultra High Temperature Ceramics for Hypersonic Vehicle Applications, Edited by Sandia National Laboratories Albuquerque, New Mexico 87185 and Livermore, California 94550, report no. SAND2006-2925 (2006)

[7] T. Cheng, W. Li, D. Fang, Thermal Shock Resistance of Ultra-High-Temperature Ceramics Under Aerodynamic Thermal Environments, AIAA Journal 51 (2013) 840-848

[8] A. Paul, J. Binner, B. Vaidhyanathan, UHTC Composites for Hypersonic Applications, in: Ultra-high temperature ceramics : materials for extreme environment applications, edited by William G. Fahrenholtz, Eric. J. Wuchina, William E. Lee, Yanchun Zhou (Wiley 2014)

[9] C.E. Kennedy, Review of mid- to high-temperature solar selective absorber materials, Technical Report No. NREL/TP-520-31267

[10] E. Sani, L. Mercatelli, F. Francini, J.-L. Sans, D. Sciti, Ultra-refractory ceramics for high-temperature solar absorbers, Scripta Materialia, 65 (2011) 775–778

[11] E. Sani, L. Mercatelli, D. Fontani, J.-L. Sans, D. Sciti, Hafnium and Tantalum Carbides for high temperature solar receivers, J. Renewable and Sustainable Energy. 3 (2011) 063107

Paper published on:
Solar Energy Materials and Solar Cells vol. 155 (2016), pages: 368–377
DOI: 10.1016/j.solmat.2016.06.028
http://www.sciencedirect.com/science/article/pii/S0927024816302033

[12] E. Sani, L. Mercatelli, P. Sansoni, L. Silvestroni, D. Sciti, Spectrally selective ultra-high temperature ceramic absorbers for high-temperature solar plants, J. Renewable and Sustainable Energy 4 (2012) 033104

[13] E. Sani, L. Mercatelli, D. Jafrancesco, J.-L. Sans, D. Sciti , Ultra-High Temperature Ceramics for solar receivers: spectral and high-temperature emittance characterization, J. European Optical Society: Rapid Publication 7 (2012) 12052

[14] D. Sciti, L. Silvestroni, L. Mercatelli, J.-L. Sans, E. Sani, Suitability of ultra-refractory diboride ceramics as absorbers for solar energy applications, Solar Energy Materials and Solar Cells 109 (2013) 8-16

[15] E. Sani, L. Mercatelli, J.-L. Sans, L. Silvestroni, D. Sciti, Porous and dense Hafnium and Zirconium Ultra-High Temperature Ceramics for solar receivers, Optical Materials 36 (2013) 163–168.

[16] E. Sani, M. Meucci, L. Mercatelli, D. Jafrancesco, J.-L. Sans, L. Silvestroni, D. Sciti, Optical properties of boride ultrahigh-temperature ceramics for solar thermal absorbers, J. Photonics for Energy 4 (2014) 045599

[17] D. Sciti, L. Silvestroni, J-L Sans., L. Mercatelli, M. Meucci, E. Sani, Tantalum diboride-based ceramics for bulk solar absorbers, Solar Energy Materials and Solar Cells, 130 (2014) 208-213

[18] D. Sciti, L.Silvestroni, D.M.Trucchi, E.Cappelli, S.Orlando, E.Sani, Femtosecond laser treatments to tailor the optical properties of hafnium carbide for solar applications, Solar Energy Materials and Solar Cells 132 (2015) 460–466

[19] E. Sani, E. Landi, D. Sciti, V. Medri, Optical properties of ZrB_2 porous architectures, Solar Energy Materials and Solar Cells, 144 (2016) 608-615

[20] E. Sani, L. Mercatelli, M. Meucci, A. Balbo, C. Musa, R. Licheri, R. Orrù, G. Cao, Optical properties of dense zirconium and tantalum diborides for solar thermal absorbers, Renewable Energy, 91 (2016) 340-346

[21] M. Romero, A. Steinfeld, Concentrating solar thermal power and thermochemical fuels, Energy Environ. Sci., 5 (2012) 9234

[22] T. Fend, B. Hoffschmidt, R. Pitz-Paal, O. Reutter, P. Rietbrock, Porous materials as open volumetric solar receivers: Experimental determination of thermophysical and heat transfer properties, Energy 29 (2004) 823-833

[23] C.C. Agrafiotis, I. Mavroidis, A. G. Konstandopoulos, B. Hoffschmidt, P. Stobbe, M. Romero, V. Fernandez-Quero, Evaluation of porous silicon carbide monolithic honeycombs as volumetric receivers/collectors of concentrated solar radiation, Solar Energy Materials and Solar Cells, 91 (2007) 474-488

[24] J. Karni, A. Kribus, R. Rubin, P. Doron, The “porcupine”: a novel high-flux absorber for volumetric solar receivers, ASME. J. Sol. Energy Eng. 120 (1998) 85-95

[25] D. Sciti, L. Silvestroni, V. Medri, F. Monteverde, Sintering and densification mechanisms of ultra-high temperature ceramics, in: Ultra-high temperature ceramics : materials for extreme environment applications, edited by William G. Fahrenholtz, Eric. J. Wuchina, William E. Lee, Yanchun Zhou (Wiley 2014)

[26] L. Silvestroni, H-J. Kleebe, S. Lauterbach, M. Müller, D. Sciti, Transmission Electron Microscopy on Zr- and Hf-borides with $MoSi_2$ addition: Densification Mechanisms, J. Material Research 25 (2010) 828-834

[27] D. Sciti, L. Silvestroni, A. Bellosi, Fabrication and properties of HfB_2-$MoSi_2$ composites produced by hot pressing and spark plasma sintering, J Material Research 21 (2006) 1460-1466.

Paper published on:
Solar Energy Materials and Solar Cells vol. 155 (2016), pages: 368–377
DOI: 10.1016/j.solmat.2016.06.028
http://www.sciencedirect.com/science/article/pii/S0927024816302033

[28] G. J. K. Harrington, G. E. Hilmas, Thermal Conductivity of ZrB_2 and HfB_2, in: Ultra-high temperature ceramics : materials for extreme environment applications, edited by William G. Fahrenholtz, Eric. J. Wuchina, William E. Lee, Yanchun Zhou (Wiley 2014)

[29] S. Chakraborty, D. Debnath, A. R. Mallick, P. K. Das, Mechanical, Tribological, and Thermal Properties of Hot-Pressed ZrB_2-B_4C Composite, Int. J. Appl. Ceram. Technol., 12 (2015) 568-576

[30] E. Zapata-Solvas, D.D. Jayaseelan, P.M. Brown, W.E. Lee, Thermal properties of La_2O_3-doped ZrB_2- and HfB_2-based ultra-high temperature ceramics, J. European Ceramic Society, 33 (2013) 3467-3472

[31] E. W. Neuman, G. E. Hilmas, Mechanical Properties of Zirconium-Diboride Based UHTCs, in: Ultra-high temperature ceramics : materials for extreme environment applications, edited by William G. Fahrenholtz, Eric. J. Wuchina, William E. Lee, Yanchun Zhou (Wiley 2014)

[32] C. M. Carney, T. S. Key, Comparison of the oxidation protection of HfB_2 based ultra-high temperature ceramics by the addition of SiC or $MoSi_2$, in "Developments in Strategic Materials and Computational Design V", Ceramics Engineering and Science Proceedings vol 35, Issue 8 (2014), 261; edited by W. M. Kriven, D. Zhu et al.

[33] E. Zapata-Solvas, D.D. Jayaseelan, P.M. Brown, W.E. Lee, Effect of La_2O_3 addition on long-term oxidation kinetics of ZrB_2–SiC and HfB_2–SiC ultra-high temperature ceramics, J. European Ceramic Society, 34 (2014) 3535-3548

[34] E. Sani, L. Mercatelli, M. Meucci, A. Balbo, L. Silvestroni, D. Sciti, Compositional dependence of optical properties of zirconium, hafnium and tantalum carbides for solar absorber applications, Solar Energy 131 (2016) 199-207

[35] L. Silvestroni, C. Melandri, S. Guicciardi, D. Sciti, TaB_2-based ceramics: microstructure, mechanical properties and oxidation resistance, J. European Ceramic Society 32 (2012) 97–105

[36] L. Silvestroni, D. Sciti, Sintering Behavior, Microstructure, and Mechanical Properties: A Comparison among Pressureless Sintered Ultra-Refractory Carbides, Advances in Materials Science and Engineering. Volume 2010 (2010), Article ID 835018, 11 pages,

[37] C. F. Bohren and D. R. Huffman, Absorption and Scattering of Light by Small Particles (Wiley, New York, 1983), pages 243-244

[38] Standard Tables for Reference Solar Spectral Irradiances: Direct Normal and Hemispherical on 37° Tilted Surface, Active Standard ASTM G173. ASTM G173–03(2012)